OECD MCCI Project

Small-Scale Water Ingression and Crust Strength Tests (SSWICS)

SSWICS 11 Design Report

Rev. 0 - FINAL

August, 2008

by:

S. Lomperski, M. T. Farmer, D. Kilsdonk, R. Aeschlimann

Reactor Analysis and Engineering Division
Argonne National Laboratory
9700 S. Cass Avenue
Argonne, IL 60439
USA

Table of Contents

1. Introduction

During the course of the first MCCI program (MCCI-1), seven small-scale water ingression tests were performed with 75 kg corium melts made up of UO_2 and varying amounts of either siliceous or limestone common sand concrete. The concrete contents varied from a low of 4 wt% to a high of 23 wt%. These tests demonstrated that melt cooling can be enhanced by water ingression made possible by thermal stress-induced cracking, and that the role of water ingression increases with decreasing concrete content. The dependence of the water ingression cooling rate on concrete content is strongest for melts containing less than 14% concrete. For melts with 14% or more concrete, little evidence of water ingression cooling was discernible. It was also found that melts with siliceous concrete cooled at about the same rate as melts with a similar amount of limestone common sand concrete.

One aim of the current MCCI program (MCCI-2) is to investigate the role of gas sparging on the corium cooling rate. The gases are a byproduct of the decomposition of concrete, which occurs when the material overheats. Gases generated near the corium/concrete interaction zone at the bottom of the melt are propelled up through the corium by buoyancy forces and the resultant gas flow has the potential to create melt porosity. This porosity is expected to supplement the fissures induced by thermal stress cracking. It is thought that these extra pathways could enhance the amount of water ingression cooling and quench the melt more rapidly than the case without sparging gases.

The first test of the MCCI-2 program was SSWICS-8, a melt quench experiment that duplicated the conditions of SSWICS-6 while adding gas sparging to simulate the flow of concrete decomposition gases. The melts for these tests were formulated to simulate a fully oxidized PWR corium melt containing 15 wt% siliceous concrete. They were both quenched at a system pressure of 1 bar. The new data was to be used to make a comparison between the cooling rates and crust morphologies of corium quenched with and without sparging gases. SSWICS-8 was an operational success in every respect except for the fact that the injected gas appeared to bypass the melt by escaping through the basemat/liner joint and/or flowing up around the melt between the melt/liner interface [1]. Post test examinations of the ingot and a review of the data determined that SSWICS-8 was effectively a repeat of SSWICS-6, i.e., a melt quenched in the absence of sparging gases. SSWICS-11, the subject of this report, will be a repeat of SSWICS-8 with a modified sparging system that is designed with the goal of ensuring that the injected gas does not bypass the melt.

This report describes the gas injection system to be used for SSWICS-11 along with test conditions and a summary of the test procedure. The report first revisits much of the design rationale for the gas sparging system that was detailed in the SSWICS-8 report. The reason for including the material again here is that, assuming this test is successful, there will be little inclination to refer to the earlier report for design background since that test was effectively one without gas sparging. Therefore all potentially pertinent material will be included in this single report. The next section describes the gas sparging system for SSWICS-11 by beginning with the design rationale for the system used in SSWICS-8.

2. Specifications for gas sparging

The main modification made to the test apparatus for SSWICS-8 was the addition of a sparging (gas injection) system able to provide a steady, controlled flow of argon gas to the basemat region immediately below the melt. The flow must be evenly distributed around the bottom of the melt and the available range of flow rates should correspond to the range predicted for the decomposition gases generated during a molten corium/concrete interaction. These requirements drove the design of the sparging system and the next portion of this section details the basis for the chosen flow range and distribution geometry.

The target midrange flow rate for the system is based on the superficial gas velocities observed in the ACE/MCCI experiments in which concrete ablation rates were measured for a variety of concrete types and melt compositions [2]. The experiments were used to investigate thermal hydraulic and chemical processes of MCCIs. They were conducted at atmospheric pressure with melt temperatures in the range of 1600-2200^{o}C. The gas generation rates varied with both concrete and melt composition. Of those tests that generated particularly high gas flows, the measured superficial gas velocities (total volumetric flow rate of gas divided by the concrete surface area) fell in the range of roughly 5-20 cm/s. These tests lasted no longer than 1 hour. The longer term tests, which lasted roughly 2 hours, generated less gas with measured velocities of 1-5 cm/s. On the basis of these experimental findings, the target midrange flow rate for the SSWICS sparging system was set at a superficial gas velocity of ~5 cm/s at a temperature of ~2000^{o}C and pressure of 1 bar.

The SSWICS MgO crucible has a cross sectional area of 0.07 m^2 and so a volumetric flow rate of 3.5e-3 m^3/s (210 liters/min) is necessary to generate a gas velocity of 5 cm/s. This midrange gas velocity is assigned to the typical initial melt temperature of ~2000^{o}C. The corresponding flow rate for the flow meter operating at room temperature is ~28 liters/min. If argon is used to simulate the decomposition gases, the mass flow rate is 0.7 g/s

The second design consideration for the injection system is the geometry of the flow delivery system. Ideally, gas flow would be evenly distributed around the bottom of the melt in an approximation of the sort of distribution one could expect from decomposing concrete. The delivery system could consist of either an array of small tubes or needles, or a porous plate, which has the potential to produce a more homogeneous gas distribution. Gas injection with the porous plate is problematic, however, under the severe operating conditions of these tests. Molten corium has the potential to clog regions of the porous plate and so it would be difficult to ensure a well-defined gas distribution under actual operating conditions. A tube array, on the other hand, can be used to produce a very well-defined gas distribution. A major advantage of an injection system based on tubes is that it can be made entirely of stainless steel and designed to operate with a large pressure drop at normal operating flow rates, which promotes stability. In contrast, it is difficult to find a porous plate with the right size, material, and required flow/ΔP characteristics. Finally, a good seal must be maintained around the porous plate to prevent bypass leakage and this would be difficult to achieve over the large operating temperature range of a typical test. Given the advantages of a tube array over a porous plate, the tube array has been chosen for the gas delivery system.

With the tube array chosen over the porous plate, it becomes necessary to select an appropriate pitch for the array. The system may, in principle, be designed with any number of tubes as long as the gas is distributed evenly among them. It is suggested that, ideally, the tubes should be close enough to effectively mimic the distribution of gas expected at the corium/concrete interface during an MCCI. Since the gases are the result of thermal decomposition of the concrete, one could expect them to be produced over the entire concrete surface. The bubbles that form at the interface and eventually release into the melt may be preferentially created at specific nucleation sites, but it is likely that the location of these sites changes as the concrete erodes. In addition, any gas film that forms over the concrete is also likely to be unstable. Given such chaotic conditions at the concrete/melt interface, it is suggested that the gas injection system will effectively mimic the source of decomposition gases in an MCCI as long as the distance between tubes is less than the typical bubble diameter. With these point sources located within a bubble diameter of one another, neighboring bubbles can coalesce or break apart as determined by factors such as flow rate and fluid physical properties. The tube spacing in this case should not have more than secondary influence on the creation of melt porosity.

An estimate of the typical bubble diameter can be obtained from the aforementioned ACE experiments. A view of the corium surface was videotaped during several tests and it was observed that

bubbles breaking through the surface had a typical diameter of the order of 50 mm [3]. The melt compositions and temperature ranges of the experiments are generally similar to those of the SSWICS experiments and so it is expected that the bubble diameters would also be similar. The ACE test results were used as part of the basis for defining the geometry of the gas injection system for the MSET-1 experiment. The MSET-1 injector was a plate with 1 mm i.d. holes arranged on a square pitch of 38 mm, which produced a hole density of ~7 holes/100 cm^2 [4].

3. Gas sparging system description

This MSET-1 injector spacing was selected for the SSWICS-8 injector since it is less than the expected bubble diameter. Figure 1 provides a top view of the basemat showing the capillary layout. A total of 44 capillaries were used, each having an inner and outer diameter of 0.57 and 1.5 mm, respectively. The capillaries are all linked to a common plenum. The reason for using capillaries in this fashion is that the system can generate low flow rates with relatively high pressure drops. A high pressure drop reduces flow fluctuations associated with changes in the downstream (RV) pressure, which can vary with, for example, liquid level. An equal flow distribution is achieved by simply matching the capillary lengths.

The tips of the capillaries were made flush with the basemat surface. It was deemed pointless to extend them above the basemat and into the melt since the initial thermite temperature is 2000°C and steel melts at 1400°C. Unfortunately, with the capillary tips located exactly at the bottom of the melt, gas was able to move laterally across the basemat and escape without passing through the melt. It is thought that shortly after thermite ignition a thin crust quickly formed between the melt and the basemat, preventing gas flow up through the melt [1].

The new configuration for SSWICS-11 introduces tubes that extend 5 cm above the basemat and into the 15 cm-deep melt. An isometric view of the layout is shown in Fig. 2. Because the initial temperature of the corium is so high, the tubes must be made of a refractory material. Ceramics are unlikely to withstand the thermal shock of thermite ignition and so tungsten has been selected. The tubes have an

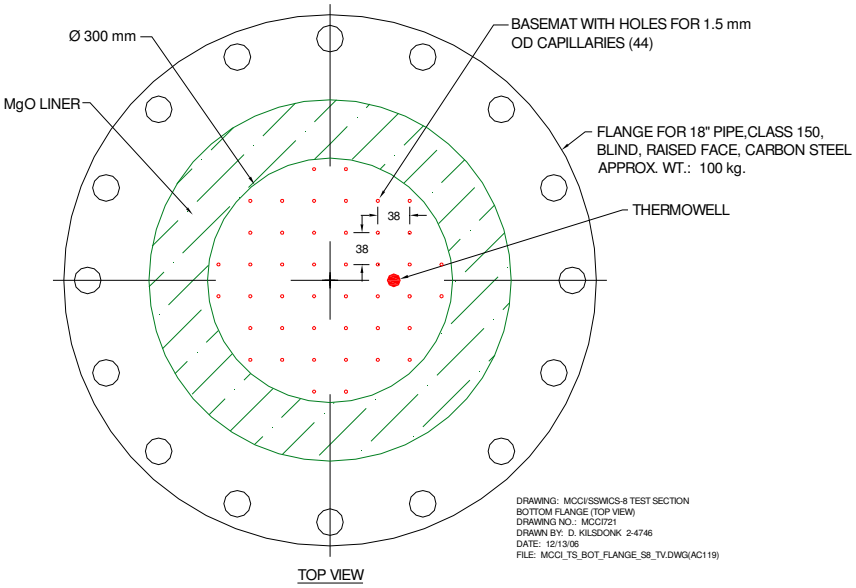

Fig. 1. SSWICS-8 capillary layout; capillary tips flush with basemat surface (dimensions in mm).

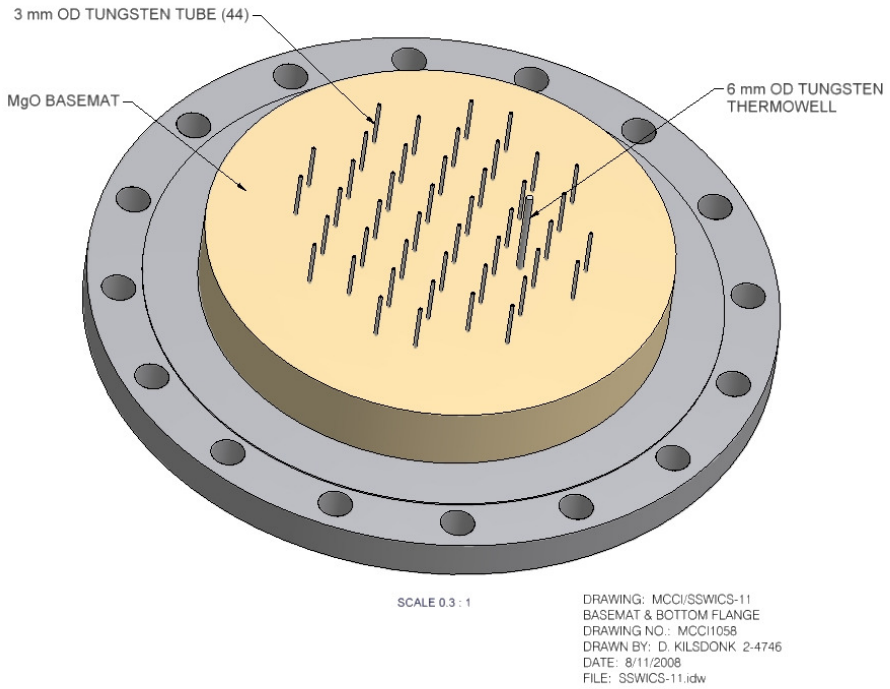

Fig. 2. SSWICS-11 tungsten tube layout with liner omitted (array pitch identical to that of SSWICS-8).

outer diameter of 3 mm (1/8”), which is the smallest available for tubes of sufficient length to extend down through the basemat, the flange, and the compression fitting. The inner diameter is 1.6 mm (1/16”). As in SSWICS-8, the total number of tubes is 44 and the pitch 38 mm. A Swagelok fitting connects each tube to a capillary (Fig. 3). The capillaries and the gas supply system are the same as those used for SSWICS-8.

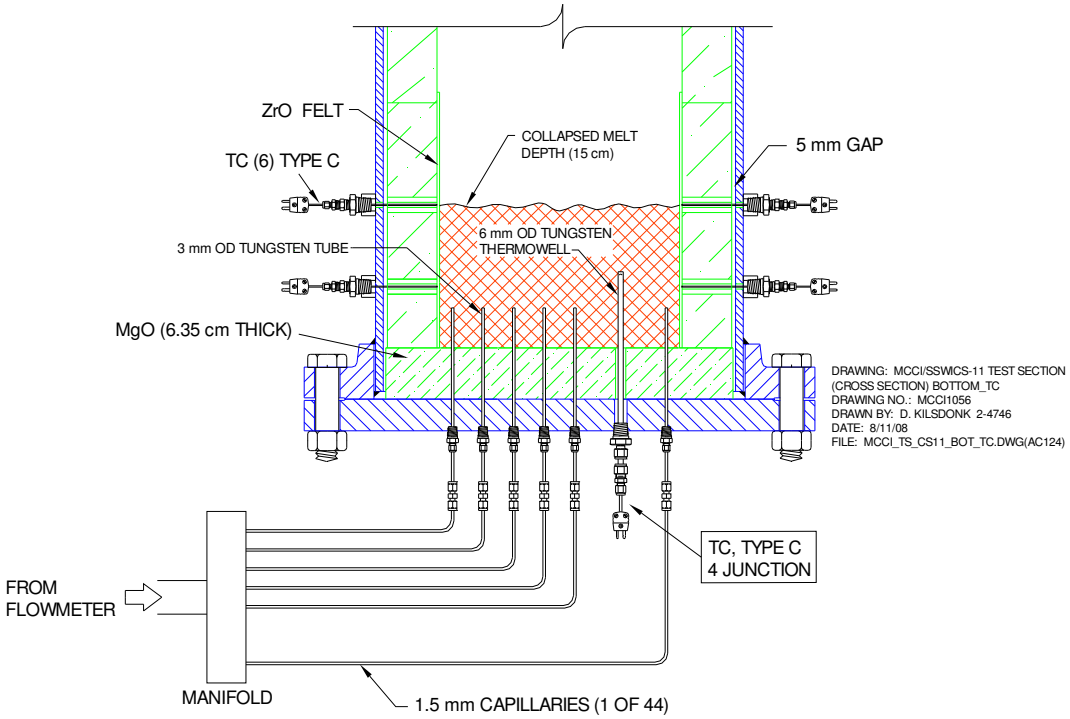

Fig. 3. Sparging system side view.

Once the melt is created from the thermite, the tubes will act as cooling fins drawing heat down into the flange to increase undesired heat losses. These new losses are acceptable, however, if they are small compared to the melt/coolant heat transfer rate. If the losses are too high, the number of tubes used in the sparging system must be reduced.

An upper limit on the losses into the flange can be estimated by considering 1-D heat transfer along a rod having a cross sectional area equivalent to that of all 44 tube walls. The heat transfer area associated with a single tube is 6e-6 m^2. The conductivity of tungsten is roughly 150 W/mK. The maximum heat flux would be observed early in the transient, when the melt is near a temperature of 2000°C and the flange less than 100°C. The distance between the bottom of the melt and the compression fitting holding the tube is ~100 mm, which is taken to be the length of the hypothetical rod. With these assumptions, the heat flux through the rod is ~3 MW/m^2 and the power drawn from the melt and deposited into the flange is ~800 W.

This upper limit 800 W heat loss is most readily compared with the melt/coolant heat transfer rate by dividing by the melt surface area scaling factor of 0.07 m^2 so that the scaled heat losses may be directly compared with the melt surface heat fluxes measured in previous tests. These are plotted in Fig. 4. It is evident from the figure that heat losses associated with the tubes are much less than the melt surface heat flux. Though the temperature gradient across the tubes is high, the total heat transfer area associated with them is quite small and so the total heat flux into the flange is acceptably low.

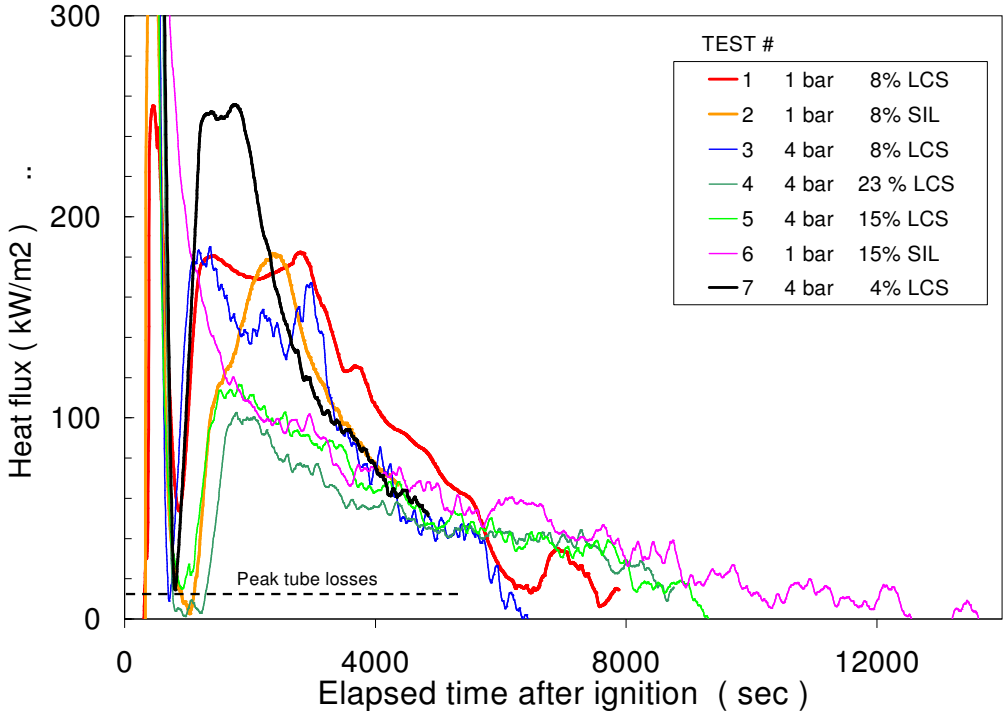

Fig. 4. Comparison between melt surface heat flux and total losses through tungsten tubes.

4. Sparging system limitations

The sparging system as designed has two particular characteristics that should be noted: 1) the system delivers gas at a constant mass flow rate rather than at a constant melt superficial velocity, and 2) the gas is not preheated before injection. This section describes how these characteristics influence the gas sparging test.

A key specification for a gas sparging test is the gas injection rate. This parameter is most conveniently defined in terms of a melt superficial gas velocity. The approach has then been to specify a particular superficial gas velocity to be established at the very beginning of a test. The flow controller is then set to deliver a constant volumetric flow rate of room temperature gas that produces the desired initial test condition. The flow controller set point is calculated with the assumption that the injected gas will be instantaneously heated to the melt temperature. The initial condition for SSWICS-8 was 2 cm/s at the beginning of the test with a presumed initial melt temperature of 2000°C. The flow controller was set to a constant 11 slpm (standard liters/minute).

The flow controller effectively maintains a constant mass flow rate and so, as the melt cools, the superficial gas velocity drops as the melt cools. Figure 5 illustrates the velocity drop that can be expected if the test is run with an initial superficial gas velocity of 5 cm/s. By the end of the test, when the melt has cooled to 100°C, the gas velocity will have dropped by a factor of six to 0.8 cm/s. Though this is a large change, much of it may be irrelevant with regards to the creation of melt porosity. Figure 5 indicates the lower limit melt solidus temperature typical of these melts. Below ~1100°C, when the melt is completely solid, the gas cannot influence the corium permeability. The plot shows that between the initial temperature of 2000°C and the solidus limit of 1100°C, the superficial velocity drops only 40% from 5 to 3 cm/s. In summary, one should be aware that the sparging system does not maintain a constant superficial gas velocity throughout a test. Also, there is a large drop in velocity over the course of a test, but much of it occurs after the melt has solidified.

Some consideration has been given to preheating the gas before it is injected into the melt. Raising the gas temperature to that of the melt would eliminate cooling that should, for the benefit of the heat flux

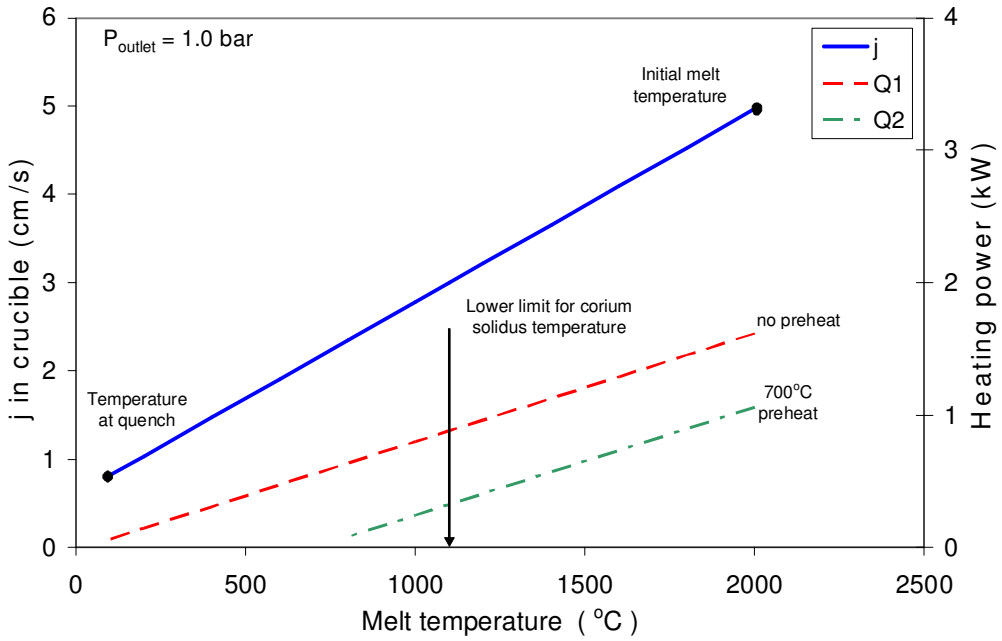

Fig. 5. Melt temperature dependence of superficial velocity and power necessary for gas preheating.

measurement, be limited to the overlying liquid layer. The thermal power needed to heat the gas from room temperature to the melt temperature has been calculated for the system midrange superficial gas velocity of 5 cm/s. The power is a function of melt temperature and so it is convenient to plot it along with the superficial gas velocity in Fig. 5. The plot shows that the maximum required power is 1.6 kW at the initial melt temperature of 2000°C, declining to less than 1 kW at the solidus temperature of 1100°C. This can be compared with typical melt cooling rates during past tests: ~10 kW shortly after water has been added to the melt and ~3-4 kW by the time the temperature drops to ~1000°C. Thus the thermal power heating the gas from room temperature to the melt temperature is expected to be equivalent to, very roughly, ~15% of the initial cooling power via surface boiling, increasing to ~25% as the melt reaches the solidus temperature (one can also scale the losses by the corium surface area and compare in Fig. 4). These loss levels demonstrate that cold gas injection would provide a significant source of melt cooling.

Gas preheating would indeed reduce the role of gas injection in melt cooling as well as its contribution to uncertainties in the measured melt surface heat flux. However, a preheat system would significantly complicate the injector design and test operation. Consider a system designed to raise the gas temperature to ~700°C, which would require a regulated heating chamber placed upstream of the inlet plenum for the capillaries. The collection of 44 capillaries would have to be insulated to maintain the gas temperature as the gas flows from the preheater to the RV. The capillaries and associated insulation can not be fully preheated before a test because of proximity to the RV bottom flange and the risk of prematurely igniting the thermite. Therefore the temperature of the gas delivered to the RV will, for some undetermined time early in the transient, be below the target temperature as the gas heats the capillaries, insulation, fittings, and bottom flange.

The installation and operation of a high temperature gas preheating system would be challenging, but feasible. It is therefore of interest to quantify the potential gains of preheating the gas to, for example, 700°C, which is an approximate upper bound for a preheating system that does not require exotic equipment. Figure 5 shows the thermal power the gas absorbs from the melt after being preheated to 700°C. This can be compared directly with the plot for gas entering the RV at room temperature. The graph shows that at the outset of a test, when the melt temperature is ~2000°C, the preheated gas absorbs about 1 kW versus 1.6 kW for the gas injected at ambient temperature. At 1000°C, the power levels are 0.3 kW versus 0.9 kW. We find this to be a rather modest reduction considering the effort required to build the preheater and the risk of operational failure. In summary, the extraneous cooling associated with room temperature gas injection amounts to only a modest fraction of the power associated with quenching. Also, a practical preheat system would achieve only a modest reduction in the gas cooling effect. For these reasons the injector does not include a preheater.

5. Test apparatus

The SSWICS reaction vessel (RV) has been designed to hold up to 100 kg of melt at an initial temperature of 2500°C. The RV lower plenum consists of a 67.3 cm long, 45.7 cm (18") outer diameter carbon steel pipe (Fig. 6). The pipe is insulated from the melt by a 6.4 cm thick layer of cast MgO. The selected pipe and insulation dimensions result in a melt diameter of 30.5 cm and a surface area of 730 cm^2. The melt depth at the maximum charge of 100 kg is about 20 cm.

The RV lower flange is insulated with a 6.4 cm thick slab of cast MgO that spans the entire inner diameter of the pipe. The MgO slab and sidewalls form the crucible containing the corium. This particular geometry was chosen to facilitate removal of the slab for the crust strength measurement tests. Corium has a tendency to bond with the MgO insulation and this design allows one to pry the slab away from the MgO walls without damaging the crust.

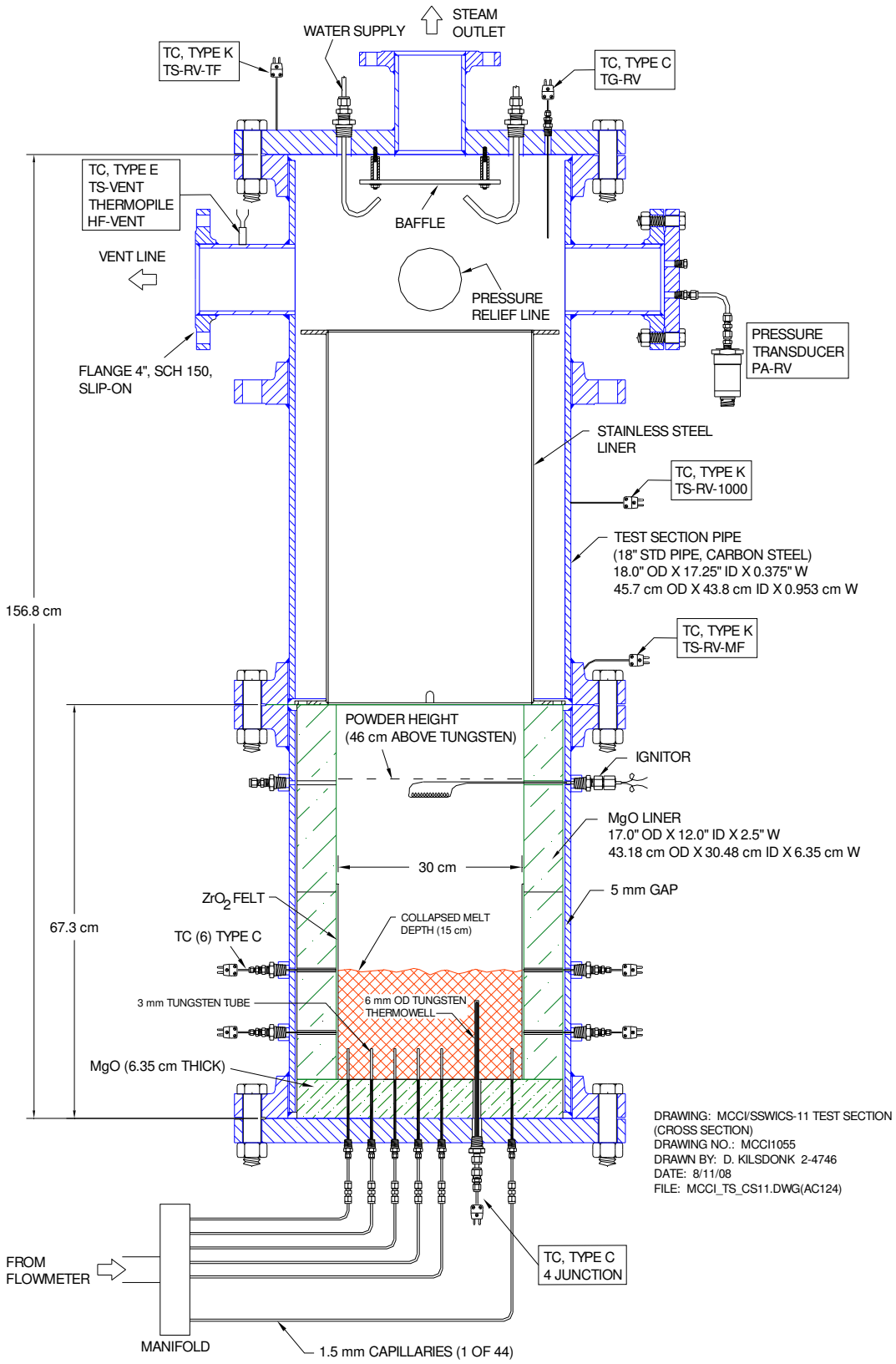

Fig. 6. Side view of SSWICS reaction vessel for dryout heat flux measurements.

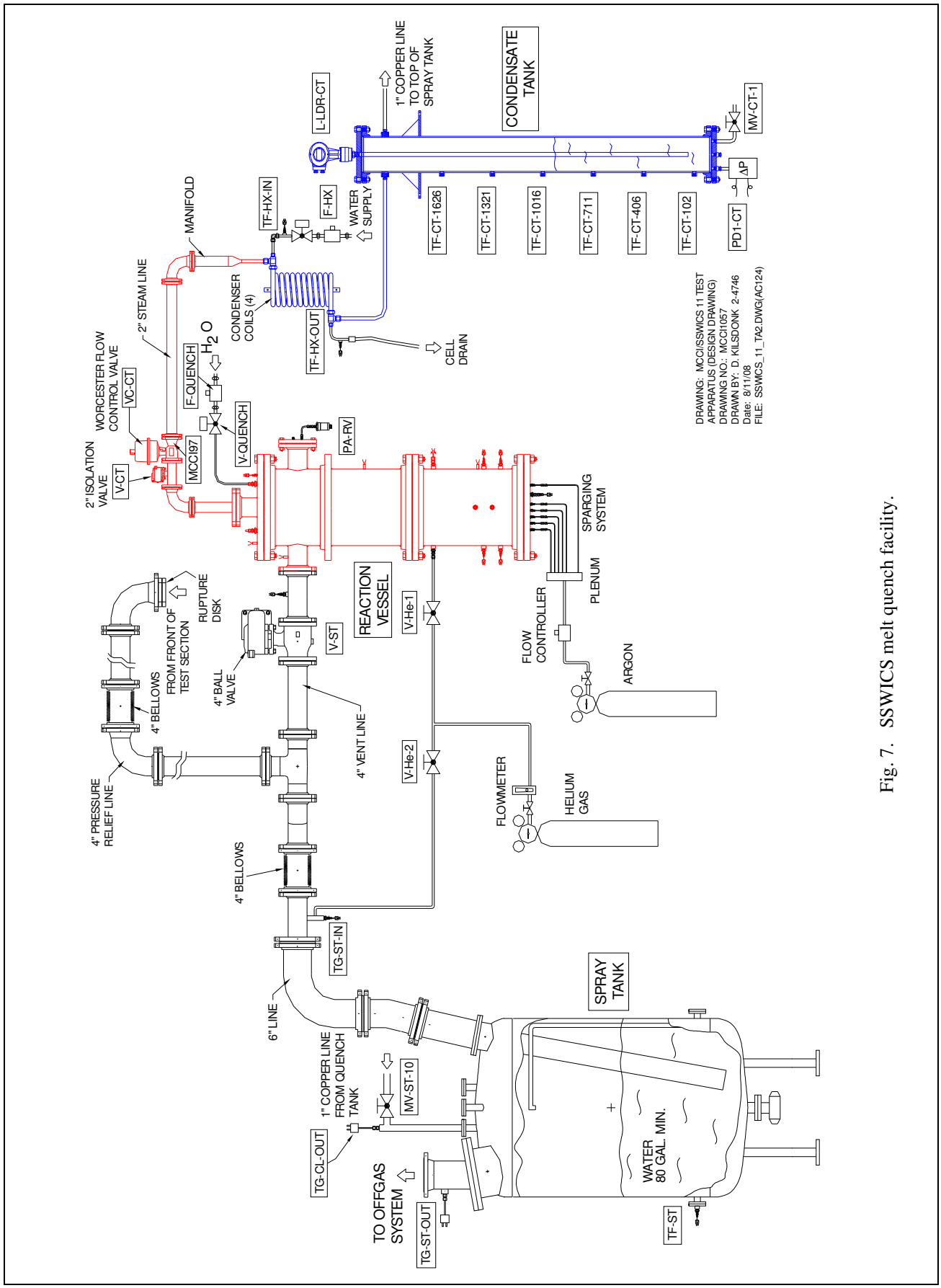

Fig. 7. SSWICS melt quench facility.

The RV upper plenum consists of a second section of pipe lined with stainless steel. The role of this liner is to protect the walls of the reaction vessel upper plenum from the heat of thermite ignition. Three 10 cm pipes welded near the top of the vessel provide 1) a vent line for the initial surge of hot noncondensable gases generated by the thermite reaction, 2) a pressure relief line with a rupture disk (7.7 bar at 100°C), and 3) an instrument flange for the absolute pressure transmitter that measures the reaction vessel pressure. Four 6 mm (¼") tubes serve as water inlets for melt quenching. A baffle is mounted below the upper flange and the water flow is directed towards the baffle to reduce the momentum of the fluid before it drops down onto the melt. The baffle is also intended to prevent water droplets from being carried up towards the condenser, which would adversely affect the heat flux measurement. A fourth 10 cm pipe welded to the top flange provides an outlet to carry steam from the quenching melt to four cooling coils. A control valve on the line allows pressure regulation for tests carried out at elevated pressure. The water-cooled coils are used to condense the steam flowing from the RV, and the condensate is collected within a 200 cm high, 20 cm diameter condensate tank (CT). Figure 7 is a schematic that provides an overview of the entire SSWICS melt-quench facility.

6. Instrumentation

Instrumentation was selected to provide the measurements necessary to determine the melt dryout heat flux. The critical measurement for these tests is the steaming rate in the RV, which is found indirectly by measuring the rate of condensate collection in the CT. A differential pressure sensor is used as the primary sensor for measuring the inventory of the condensate tank while a time domain reflectometer provides a supplementary level measurement.

The melt temperature is measured with a multi-junction probe made up of 4 C-type (W-5%Re/W-26%Re) thermocouples (Fig. 8). The probe is mounted on the bottom flange of the RV and protected from the melt by a tungsten thermowell. The thermowell has a 6 mm o.d. and 1 mm wall, and the top end is positioned 100 mm above the bottom of the melt. The thermocouples are located 100, 80, 60, and 40 mm above the bottom of the melt.

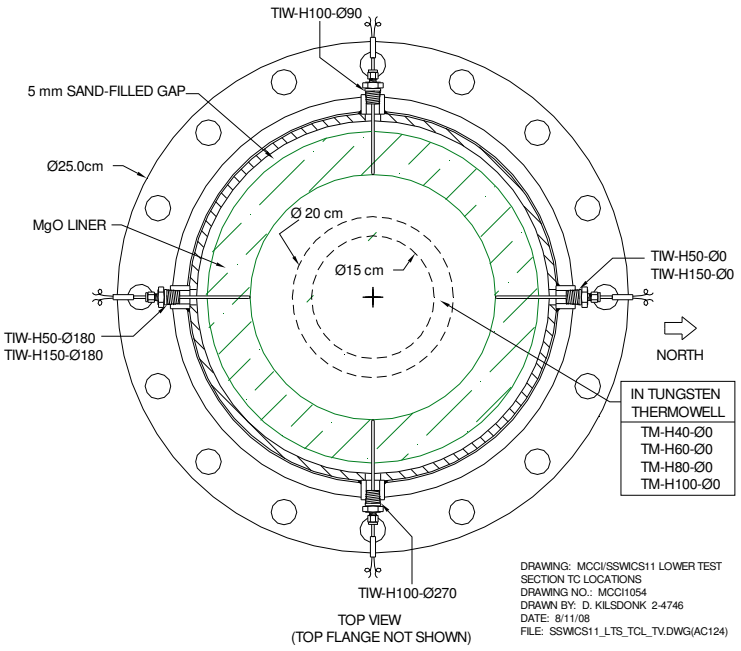

Fig. 8. Instrumentation positions in basemat and lower MgO liner.

Six C-type thermocouples are used to measure temperatures at the corium/lining interface to show whether water seeps around the edges of the melt to provide unwanted lateral cooling. Two thermocouples are positioned 150 mm above the base of the melt, two at 100 mm, and two at 50 mm.

7. Data acquisition and control systems

All data acquisition and process control tasks are managed by a PC executing LabVIEW 6.i under Windows XP. Sensor output terminals are connected to model HP E1345A 16-channel multiplexers and the signals are digitized by an HP E1326B 5 ½ digit multimeter located within the test cell (Fig. 10). Signal noise is reduced by integration over a single power line cycle (16.7 ms). The digitized sensor readings are routed from the test cell to the PC in the control room via two HP-IB extenders. The extenders allow the ASCII data from the HP to be sent through the cell wall over a BNC cable. The extender within the control room then communicates with a GPIB card within the PC. This configuration also permits remote control of the multimeter through LabVIEW. The power line cycle integration results in a minimum (theoretical) time of 0.75 s to scan the channel list (16.7 ms * 45 channels). In practice, however, the acquisition of a single scan is at a frequency of approximately 0.5 Hz.

Valves are controlled with the PC using a relay card housed within an SCXI chassis (National Instruments). These electromechanical relays are capable of switching up to 8 A at 125 VAC or 5 A at 30 VDC. They are operated via a switch controller in the SCXI chassis, which communicates with the PC through a general-purpose data acquisition card. As shown in Figure 9, the relays in the control room operate devices within the test cell indirectly, through a second relay. This is intended to provide an additional level of electrical isolation between the NI switching hardware and high voltage sources within the cell. As an added safety measure, all wiring is routed through a control panel that can be switched from automatic (PC) control to manual control in the event of computer failure. A complete instrument list is provided in Table 1.

8. Test parameters

The test parameters of SSWICS-11 will duplicate those of SSWICS-8. The melt composition will be the same as that of both SSWICS-8 and SSWICS-6, which was used to investigate the quenching behavior of a fully oxidized PWR corium melt containing 15 wt% siliceous concrete at a system pressure of 1 bar absolute. It was the only test in which the RV was heated to the saturation temperature to completely eliminate undesirable structure heating during the early portion of the transient. As a result, the overall energy balance for SSWICS-6 was superior to the other six tests and so it is the best base case with which to compare a new test with gas injection.

The thermite and corium compositions planned for SSWICS-11 are shown in Tables 2. The proposed test procedure, which is similar to that of SSWICS-8, is summarized as follows:

1) Preheat RV structures and water inventory to ~100^{o}C.
2) Arm thermite ignition system.
3) Set argon flow into injector to 11 liters/min (corresponds to 2 cm/s in RV at 2000^{o}C).
4) Ignite thermite to begin test.
5) Confirm that melt reaches target temperature of ~2000^{o}C (usually within one minute of the first sign of ignition).

6) Commence water injection at a rate of ~15 liters/min until 40 liters of water have been injected into the RV.
7) No other operator actions until corium is quenched (expected to occur more quickly than the 3.8 hours required to quench SSWICS-6).
8) The melt is considered quenched, and the test complete, when readings from all four thermocouples within the tungsten thermowell reach the saturation temperature of 100°C.

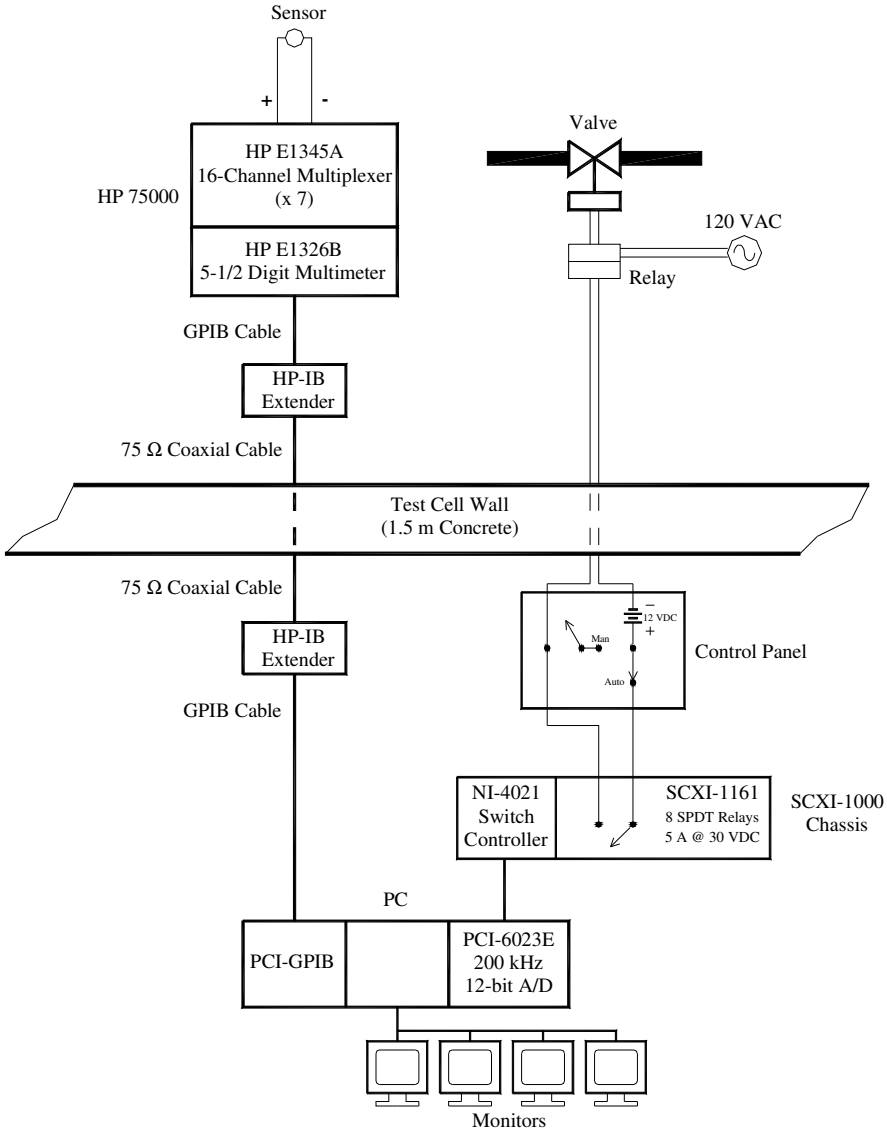

Fig. 9. Data acquisition and control systems.

#	Channel	Name	Type	Description	Serial #	Output	Range	Accuracy
0	HPS-0	T-CJ-HPS	AD592 IC	Cold junction compensation sensor.	-	1 μA/K	0-70°C	±0.5°C
1	HPS-1	TM-H100-Φ0	TC type C	Melt temp. 100 mm above bottom of melt (in tungsten thermowell).	-	0-37 mV	0-2320°C	±4.5°C or 1%
2	HPS-2	TM-H80-Φ0	TC type C	Melt temp. 80 mm above bottom of melt (in tungsten thermowell).	-	0-37 mV	0-2320°C	±4.5°C or 1%
3	HPS-3	TM-H60-Φ0	TC type C	Melt temp. 60 mm above bottom of melt (in tungsten thermowell).	-	0-37 mV	0-2320°C	±4.5°C or 1%
4	HPS-4	TM-H40-Φ0	TC type C	Melt temp. 40 mm above bottom of melt (in tungsten thermowell).	-	0-37 mV	0-2320°C	±4.5°C or 1%
5	HPS-5	Reserve	TC type C	-	-	0-37 mV	0-2320°C	±4.5°C or 1%
6	HPS-6	Reserve	TC type C	-	-	0-37 mV	0-2320°C	±4.5°C or 1%
7	HPS-7	Reserve	TC type C	-	-	0-37 mV	0-2320°C	±4.5°C or 1%
8	HPS-8	TIW-H50-Φ0	TC type C	Melt temp. at inner sidewall 50 mm above bottom of melt.	-	0-37 mV	0-2320°C	±4.5°C or 1%
9	HPS-9	TIW-H50-Φ180	TC type C	Melt temp. at inner sidewall 50 mm above bottom of melt.	-	0-37 mV	0-2320°C	±4.5°C or 1%
10	HPS-10	TIW-H100-Φ90	TC type C	Melt temp. at inner sidewall 100 mm above bottom of melt.	-	0-37 mV	0-2320°C	±4.5°C or 1%
11	HPS-11	TIW-H100-Φ270	TC type C	Melt temp. at inner sidewall 100 mm above bottom of melt.	-	0-37 mV	0-2320°C	±4.5°C or 1%
12	HPS-12	TIW-H150-Φ0	TC type C	Melt temp. at inner sidewall 150 mm above bottom of melt.	-	0-37 mV	0-2320°C	±4.5°C or 1%
13	HPS-13	TIW-H150-Φ180	TC type C	Melt temp. at inner sidewall 150 mm above bottom of melt.	-	0-37 mV	0-2320°C	±4.5°C or 1%
14	HPS-14	Reserve	TC type C	-	-	0-37 mV	0-2320°C	±4.5°C or 1%
15	HPS-15	Reserve	TC type C	-	-	0-37 mV	0-2320°C	±4.5°C or 1%
16	HPS-16	Reserve	TC type C	-	-	0-37 mV	0-2320°C	±4.5°C or 1%
17	HPS-17	Reserve	TC type C	-	-	0-37 mV	0-2320°C	±4.5°C or 1%
18	HPS-18	TG-RV	TC type C	Gas temp. in reaction vessel upper plenum.	-	0-37 mV	0-2320°C	±4.5°C or 1%
19	HPS-19	Reserve	TC type K	-	-	0-50 mV	0-1250°C	±2.2°C or 0.75%
20	HPS-20	Reserve	TC type K	-	-	0-50 mV	0-1250°C	±2.2°C or 0.75%
21	HPS-21	Reserve	TC type K	-	-	0-50 mV	0-1250°C	±2.2°C or 0.75%
22	HPS-22	TS-RV-tf	TC type K	Temperature of RV top flange.	-	0-50 mV	0-1250°C	±2.2°C or 0.75%
23	HPS-23	TS-RV-1000	TC type K	Outer wall temp. of RV 1000 mm above bottom of melt.	-	0-50 mV	0-1250°C	±2.2°C or 0.75%
24	HPS-24	TS-RV-mf	TC type K	Temperature of RV middle flange.	-	0-50 mV	0-1250°C	±2.2°C or 0.75%
25	HPS-25	TS-RV-100	TC type K	Outer wall temp. of RV 100 mm above bottom of melt.	-	0-50 mV	0-1250°C	±2.2°C or 0.75%
26	HPS-26	TS-RV-bf	TC type K	Temperature of RV bottom flange.	-	0-50 mV	0-1250°C	±2.2°C or 0.75%
27	HPS-27	TS-vent	TC type E	Outer wall temp. of vent line.	-	0-70 mV	0-900°C	±1.7°C or 0.5%
28	HPS-28	TF-CT-102	TC type K	Fluid temp. in condensate tank at a water level of 102 mm.	-	0-50 mV	0-1250°C	±2.2°C or 0.75%
29	HPS-29	TF-CT-406	TC type K	Fluid temp. in condensate tank at a water level of 406 mm.	-	0-50 mV	0-1250°C	±2.2°C or 0.75%
30	HPS-30	TF-CT-711	TC type K	Fluid temp. in condensate tank at a water level of 711 mm.	-	0-50 mV	0-1250°C	±2.2°C or 0.75%
31	HPS-31	TF-CT-1016	TC type K	Fluid temp. in condensate tank at a water level of 1016 mm.	-	0-50 mV	0-1250°C	±2.2°C or 0.75%
32	HPS-32	TF-CT-1321	TC type K	Fluid temp. in condensate tank at a water level of 1321 mm.	-	0-50 mV	0-1250°C	±2.2°C or 0.75%
33	HPS-33	TF-CT-1626	TC type K	Fluid temp. in condensate tank at a water level of 1626 mm.	-	0-50 mV	0-1250°C	±2.2°C or 0.75%
34	HPS-34	TF-HX-in	TC type K	Fluid temp. at HX coolant inlet.	-	0-50 mV	0-1250°C	±2.2°C or 0.75%
35	HPS-35	TF-HX-out	TC type K	Fluid temp. at HX coolant outlet.	-	0-50 mV	0-1250°C	±2.2°C or 0.75%

Table 1. Instrumentation list for water ingression tests (part 1 of 2).

#	Channel	Name	Type	Description	Serial #	Output	Range	Accuracy
36	HPS-36	HF-vent	Thermopile	Heat Flux through connecting line to V-ST.	0632	0-5.50 mV	0-5 kW/m^2	±3%
37	HPS-37	I-ign	DC supply	Current supply for thermite ignitor.	-	0-100 mV	0-25 Amps	-
38	HPS-38	TF-quench	TC type K	Temperature of water injected into RV	-	0-50 mV	0-1250^{o}C	±2.2^{o}C or 0.75%
39	HPS-39	Reserve	-	-	-	-	-	-
40	HPS-40	PA-RV	1810AZ	Absolute pressure in reaction vessel.	02351-00P1PM	1-6 V	0-14 bar gage	±0.14 bar
41	HPS-41	PD-CT	1801DZ	$\overline{P}$ transmitter to measure condensate inventory.	D-9	0-13 V	0-0.35 bar	±0.004 bar
42	HPS-42	L-TDR-CT	BM100A	Time domain reflectometer to measure CT level.	A02331879A	4 - 20 mA	0 - 2 m	±3 mm
43	HPS-43	VDC-P-supply	-	Voltage of the power supply for the pressure transmitters.	-	0 - 15 V	-	-
44	HPS-44	F-sparge	HFC-203	Flow rate of argon into injector for gas sparging	3621300001	0 - 5 V	0-50 sl/m Ar	±0.5 sl/m
45	HPS-45	Reserve	-	-	-	-	-	-
46	HPS-46	Reserve	-	-	-	-	-	-
47	HPS-47	Reserve	-	-	-	-	-	-
48	HPS-48	Reserve	-	-	-	-	-	-
49	HPS-49	Reserve	-	-	-	-	-	-
50	HPS-50	Reserve	-	-	-	-	-	-
51	HPS-51	Reserve	-	-	-	-	-	-
52	HPS-52	Reserve	-	-	-	-	-	-
53	HPS-53	Reserve	-	-	-	-	-	-
54	HPS-54	Reserve	-	-	-	-	-	-
55	HPS-55	Reserve	-	-	-	-	-	-
56	HPS-56	Reserve	-	-	-	-	-	-
57	HPS-57	Reserve	-	-	-	-	-	-
58	HPS-58	Reserve	-	-	-	-	-	-
59	HPS-59	Reserve	-	-	-	-	-	-
60	HPQ-50	T-CJ-HPQ	AD592 IC	Cold junction compensation sensor.	-	1 $\overline{A}$/K	0-70^{o}C	±0.5^{o}C
61	HPQ-51	TF-ST	TC type K	Fluid temp. in spray tank.	-	0-50 mV	0-1250^{o}C	±2.2^{o}C or 0.75%
62	HPQ-52	TG-CL-out	TC type K	Gas temperature in condensate tank outlet line to spray tank.	-	0-50 mV	0-1250^{o}C	±2.2^{o}C or 0.75%
63	HPQ-53	TG-ST-in	TC type K	Gas temp. in the spray tank line inlet.	-	0-50 mV	0-1250^{o}C	±2.2^{o}C or 0.75%
64	HPQ-54	TG-ST-out	TC type K	Gas temp. in the spray tank line outlet.	-	0-50 mV	0-1250^{o}C	±2.2^{o}C or 0.75%
65	HPQ-55	F-quench	Paddlewheel	Flow rate of water into reaction vessel (for quenching melt).	3144	0-5 V	0-50 gpm	±0.5 gpm
66	HPQ-56	F-HX	Paddlewheel	Flow rate of cold water to heat exchangers.	3143	0-5 V	0-50 gpm	±0.5 gpm

Table 1. (continued).

LabVIEW Channel #	Valve Name	Description	Actuator
1	V-CT	Valve on steam line between reaction vessel and quench tank.	Pneumatic
2	V-quench	Valve on quench water supply line into reaction vessel.	Solenoid
3	V-quench-i	Isolation valve on quench water supply line into reaction vessel.	Solenoid
4	V-quench-b	Valve on back-up quench water supply.	Solenoid
5	V-ST	Valve on vent line between reaction vessel and spray tank.	Pneumatic
Panel	V-HX	Valve on cooling-water line to heat exchangers.	Solenoid
Panel	VC-CT	Control valve on steam line between reaction vessel and quench tank.	Electric

Constituent	Mass (kg)
U_3O_8	39.92
CrO_3	8.40
CaO	1.50
Zr	11.68
Mg	0.04
Si	1.08
SiO_2	5.32
Al	0.06
Total	68.0

Constituent	Wt %	
	Reactant	Product
U_3O_8	58.70	-
UO_2	-	56.32
Zr	17.16	-
ZrO_2	-	23.13
Si	1.57	-
SiO_2	7.84	11.17
Mg	0.07	-
MgO	-	0.12
Al	0.09	-
Al_2O_3	-	0.64
CaO	2.21	2.21
CrO_3	12.36	-
Cr	-	6.41

Tables 2. Corium powder charge and reaction product mass fractions.

9. References

[1] S. Lomperski, M. T. Farmer, D. J. Kilsdonk, and R. W. Aeschlimann, *Small-Scale Water Ingression and Crust Strength Tests (SSWICS); SSWICS-8 Test Data Report: Thermalhydraulic Results,* OECD/MCCI-2007-TR02, Rev 2. April 2007.

[2] D. H. Thompson, M. T. Farmer, J. K. Fink, D. R. Armstrong, B. W. Spencer, *ACE phase C final report: volume I-MCCI thermal hydraulic results*, ACE_TR-C42, September 1997, page 4-5.

[2] Video archives of the ACE/MCCI program, M. T. Farmer and B. W. Spencer.

[3] M. T. Farmer, D. J. Kilsdonk, R. W. Aeschlimann, *MSET-1 test data report*, MACE-TR-D17 January 2002.

[4] M. T. Farmer and B. W. Spencer, *A review of the database pertaining to ex-vessel debris coolability*, EPRI technical report ACEX-TR-C34, February 2000.